Journal of Drug Delivery Science and Technology 119 (2026) 108113

Contents lists available at ScienceDirect

Journal of Drug Delivery Science and Technology

journal homepage: www.elsevier.com/locate/jddst

pH-responsive delivery of azelaic acid from citric acid-crosslinked hydroxypropyl methylcellulose/poly(vinyl alcohol) nanofibers

Ehsan Niknejad [a], Reza Jafari [a,*], Valeria Morales Pascal [a,b], Gelareh Momen [a,c]

[a] Department of Applied Science, University of Quebec at Chicoutimi (UQAC), 555, Boul. Université, Chicoutimi, QC, G7H 2B1, Canada
[b] Nanotechnology Engineering Program, Monterrey Institute of Technology and Higher Education, Estado de México Campus, Carretera Lago de Guadalupe Km. 3.5, Atizapán de Zaragoza, State of Mexico, 52926, Mexico
[c] Department of Engineering, École de Technologie Supérieure (ETS), Montréal, QC, H3C 1K3, Canada

ARTICLE INFO

Keywords:
HPMC/PVA nanofibers
Citric acid crosslinking
Electrospinning
pH-responsive
Azelaic acid
Controlled release

ABSTRACT

Fabricating stable, functional nanofibers from hydroxypropyl methylcellulose (HPMC) remains a significant challenge due to its poor electrospinnability and high water-solubility. This work overcomes these limitations by engineering a novel, pH-responsive platform via electrospinning HPMC with poly(vinyl alcohol) (PVA) and applying a safe, green thermal crosslinking with citric acid. This strategy converted the polymer blend from a rapidly dissolving mat into a robust, smart system. Characterization (SEM, FTIR, DSC) confirmed uniform, bead-free morphology, successful ester-bond formation, and enhanced thermal stability. Crosslinking induced a super-hydrophilic surface (WCA 16.3°), favorable for biological fluid interaction. The platform's function was demonstrated with azelaic acid (AzA), where crosslinking transformed its release profile from a rapid burst (>90% in 2 h) to a finely tuned, pH-dependent mechanism. The crosslinked mats provided a smart, sustained release: minimal at pH 4.5 (healthy skin), moderate at pH 6.0, and maximum at pH 7.4 (diseased skin), achieving over 87% release. Kinetic modeling (Korsmeyer-Peppas model) confirmed that drug transport is governed by Fickian diffusion, with the rate profoundly accelerated by pH-triggered swelling. This study establishes a scalable, biocompatible, and intelligent nanofibrous drug delivery platform for on-demand dermatological therapies and advanced wound dressings.

1. Introduction

Stimuli-responsive, or "smart," polymers alter their physical or chemical properties in response to their environment and are attracting attention across medicine [1], sensors [2], tissue engineering [3] and packaging [4]. These materials respond to triggers such as light, temperature, pH, electric/magnetic fields, and biological signals [5]. Among them, pH-responsive polymers are particularly useful because many biological microenvironments such as inflamed tissue, tumors, wounds, or the digestive tract show distinct pH differences that can be exploited for targeted delivery [6].

A pH-responsive delivery strategy has been widely explored in skin therapy, where the difference between healthy skin (pH 4.5 to 5.5) and diseased conditions such as atopic dermatitis (pH up to 7.4) can serve as a trigger for selective drug release. This approach keeps the formulation inactive on healthy skin and activates it only at diseased sites [7]. The natural pH gradient of the skin therefore acts as a non-invasive biomarker for targeted release and is an important concept in smart dermatological systems [8]. This concept is schematically illustrated in Fig. 1. Healthy skin maintains an acid mantle with a pH of 4.5 to 5.5, while conditions such as chronic wounds, acne, and eczema often show elevated pH values between 6.0 and 7.4 due to inflammation and bacterial activity [9]. This clear pH difference forms the basis of this work, which aims to design a material that remains stable at pH 4.5 but activates at higher pH to ensure localized release and reduced systemic exposure.

Two main strategies are commonly used to create pH-responsive platforms. The first relies on incorporating ionizable groups such as carboxyl or amine moieties. Their charge density changes with pH, which alters polymer swelling or shrinkage and therefore controls drug diffusion. The second strategy uses pH-labile bonds such as acetals that cleave under specific pH conditions to trigger release. These

* Corresponding author.
E-mail addresses: eniknejad@etu.uqac.ca (E. Niknejad), reza_jafari@uqac.ca (R. Jafari), A01798186@tec.mx (V.M. Pascal), gelareh_momen@uqac.ca (G. Momen).

https://doi.org/10.1016/j.jddst.2026.108113
Received 12 December 2025; Received in revised form 25 January 2026; Accepted 7 February 2026
Available online 8 February 2026

mechanisms have been applied in nanoparticles, hydrogels, membranes, and fibers, where the response can be tuned by modifying the network chemistry and crosslink density [10]. Electrospun nanofibers are particularly promising for this purpose because their high surface-to-volume ratio [11] and interconnected porosity enhance fluid permeation and allow precise control over diffusion and degradation [12,13]. Recent advancements have further expanded this versatility, demonstrating the efficacy of functionalized PVA fibers for antibacterial performance [14] and emulsion electrospinning for enhancing drug bioavailability [15], as well as the use of coaxial processing [16] and synergistic crosslinking [17] to tailor structural integrity. These capabilities make electrospun fibers well suited for pH-sensitive skin applications, where local pH shifts can be rapidly detected and used to trigger targeted release [18].

While other pH-responsive polysaccharides have been explored, they often present significant processing challenges. For instance, chitosan typically requires harsh acidic solvents for electrospinning and toxic agents like glutaraldehyde for stability [19,20]. Alginate exhibits poor spinnability due to polyelectrolyte repulsion and requires complex ionic crosslinking that often compromises fiber integrity [21]. Similarly, NaCMC is difficult to stabilize in aqueous environments without excessive loss of swelling capacity [22]. In contrast, hydroxypropyl methylcellulose (HPMC) offers distinct advantages. It is a non-ionic cellulose derivative that can be processed in both aqueous and organic solvents and forms stable films with tunable viscosity grades [23]. HPMC is biocompatible and widely used in pharmaceutical formulations such as tablets, films, and topical systems. Its abundant hydroxyl groups also allow chemical modification and crosslinking, which enables improved fiber stability and tailored functional performance after electrospinning [24]. Furthermore, unlike the aforementioned polysaccharide systems, the HPMC platform offers a fully 'green,' aqueous-based manufacturing process to create a robust, pH-gated network without relying on toxic solvents or expensive post-treatments. Compared with HPMC films, electrospun HPMC fibers disintegrate faster, release drugs more efficiently, and show higher flexibility due to their nanoscale structure [25].

Despite these advantages, HPMC is highly hydrophilic, which slows solvent evaporation during electrospinning and promotes gelation and phase separation, leading to an unstable jet and irregular fibers [26,27]. To address these challenges, researchers commonly blend HPMC with polymers such as poly(vinyl alcohol) (PVA) [28] or poly(ethylene glycol) (PEO) [29] and adjust the solvent system using mixed water and alcohol formulations [30,31]. PVA is effective because it increases viscosity and chain entanglement [32], stabilizes the jet, and produces uniform fibers [33]. Its biocompatibility and history of use in drug delivery and wound healing further support its role as a suitable partner for improving the spinnability of HPMC [34]. These formulation choices are essential for producing HPMC-based fibers suitable for biomedical and controlled release applications.

To introduce water resistance and pH responsiveness into these hydrophilic mats, thermal crosslinking with citric acid (CA) offers a safe and scalable strategy [35]. When heated between 120 and 160 °C, the hydroxyl groups of HPMC and PVA react with the carboxyl groups of CA, forming ester crosslinks that restrict chain mobility and create a stable three-dimensional network (Fig. 2). This reaction strengthens the fibers, reduces aqueous solubility, and enables pH-dependent swelling [36,37]. Such stabilization is essential for converting hydrophilic cellulose derivatives into functional fibrous systems capable of controlled and responsive drug release.

Although citric acid crosslinking has been widely applied to HPMC-based films and hydrogels [36,37], these bulk systems do not provide the high surface-to-volume ratio or interconnected porosity that define electrospun nanofibers. To the best of our knowledge, this non-toxic crosslinking strategy has not been applied to HPMC/PVA electrospun fibers to create a pH-responsive platform. By combining HPMC's

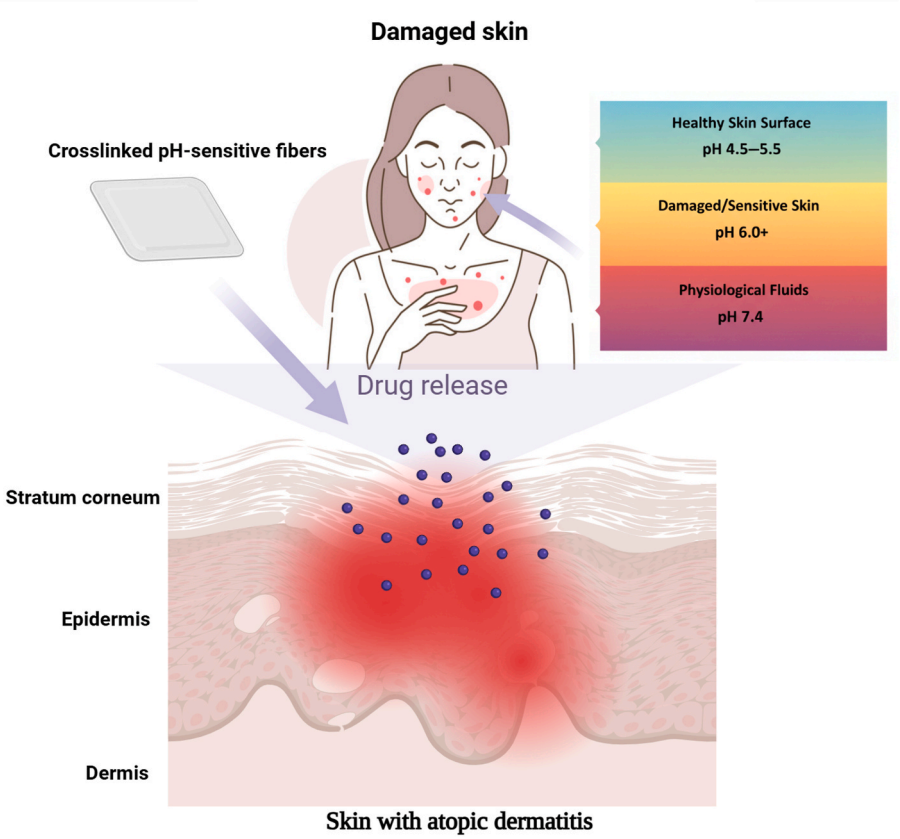

Fig. 1. The physiological pH gradient as a non-invasive biomarker for targeted delivery. The elevated pH > 6.0 in inflamed sites serves as the activation trigger for pH-responsive drug systems.

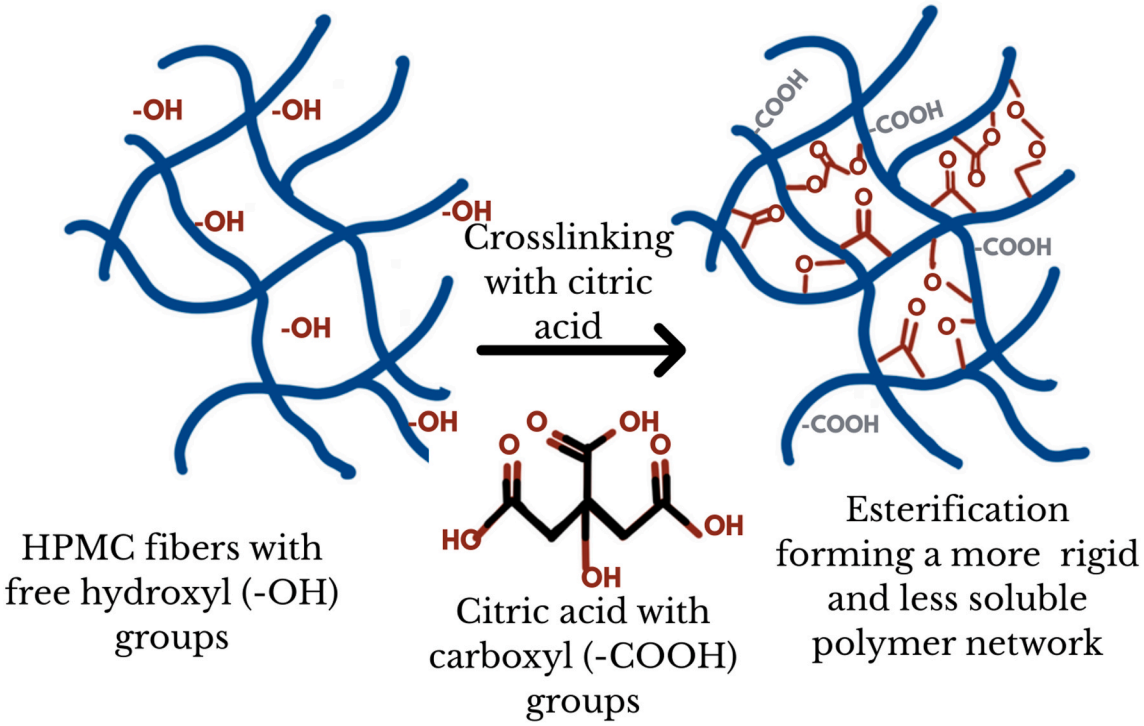

Fig. 2. Schematic of the esterification reaction between HPMC and citric acid, forming a crosslinked polymer network.

biomedical relevance with the structural advantages of nanofibers and the stabilizing effect of CA crosslinking, this work addresses a clear gap and advances HPMC toward use as a smart fibrous carrier [12].

To evaluate the pH-responsive behavior of the crosslinked mats, azelaic acid (AzA) was selected as a model drug. AzA is an FDA-approved dicarboxylic acid with antibacterial and anti-inflammatory activity and is widely used in dermatology for acne, rosacea, and hyperpigmentation [38–40]. Its pH-dependent ionization, with pKa values around 4.5 to 5.5, and its limited solubility at neutral pH make it a suitable probe to study how swelling and charge interactions influence release kinetics [40]. Using AzA therefore provides both clinical relevance and a clear method to assess the pH-sensitive release performance of the developed HPMC/PVA nanofiber system.

We hypothesize that citric acid esterification of the HPMC/PVA nanofiber matrix will form a stable, water-resistant network capable of controlled, pH-dependent azelaic acid release through the combined effects of polymer swelling and drug ionization. The motivation for this hypothesis stems from the growing demand for intelligent, stimuli-responsive pharmaceutical formulations for dermal applications. Within this context, the HPMC/PVA blend offers a promising nanomedicine platform, where the introduction of citric acid creates a pH-sensitive network that converts a rapidly dissolving matrix into a precise, pH-gated drug carrier. Such advanced delivery systems are increasingly explored for wound healing and localized dermatological therapies [41]. Guided by this hypothesis, the present work focuses on developing these crosslinked nanofibers and evaluating how chemical modification influences physicochemical stability, swelling kinetics, and stimuli-responsive release behavior. This study therefore aims to establish a scalable smart delivery platform that responds selectively to the elevated pH characteristic of diseased skin to enhance therapeutic efficacy.

2. Material and methods

2.1. Materials

Hydroxypropyl methylcellulose (HPMC, CAS No. 9004-65-3; Catalog No. 045847.22) was obtained from Thermo Scientific Chemicals (Fisher Scientific, Canada). According to the supplier, the polymer contained a methoxyl substitution of 28–30% and a hydroxypropyl substitution of 7–12%, corresponding to the established substitution pattern for this cellulose ether. The molecular weight was specified by the manufacturer through a viscosity grade of 7500–14,000 mPa s, measured for a 2% aqueous solution at 20 °C (Lot No. W03K004). These structural specifications represent the complete characterization provided by the manufacturer and determine the behavior of HPMC during electrospinning and subsequent citric acid crosslinking.

Poly(vinyl alcohol) (PVA; CAS No. 9002-89-5; Catalog No. 363154-250G) was obtained from Sigma-Aldrich with a molecular weight of 85,000–124,000 g/mol and a degree of hydrolysis of 99+% (Lot No. 03628 MC). Citric acid (CA; CAS No. 77-92-9; Catalog No. BP339-500) was purchased from Fisher Bioreagents at a purity of 99.5% (Lot No. 241980) and used as the crosslinker. Azelaic acid (AzA; CAS No. 123-99-9; Catalog No. 036308.14) was obtained from Thermo Scientific Chemicals with a purity of 98% (Lot No. 5001I24T) and served as the model drug. Ethanol (EtOH; CAS No. 64-17-5; Catalog No. C1120700-4A) was sourced from Reagents (Charlotte, NC, USA) at analytical grade purity (≥99.8%; Lot No. 44070376). All chemicals were used as received without further purification. Deionized water was used throughout the study.

2.2. Preparation of electrospinning solution

HPMC (2% w/v) was first dissolved in distilled water at 50 °C and stirred for 24 h until completely dissolved. Higher concentrations were avoided due to excessive viscosity that hindered proper mixing. This solution was further diluted with ethanol to obtain a 1% w/v HPMC solution in a 50:50 (v/v) water–ethanol mixture. Separately, PVA was dissolved in deionized water (8% w/v) at 80 °C under continuous stirring until clear and then cooled to room temperature. The two polymer solutions were then combined to obtain a final composition of 70% w/w HPMC and approximately 30% w/w PVA, relative to the total polymer content. Citric acid (0.5% w/v) was incorporated as the crosslinking agent (noting that previous studies have reported using either 0.5% w/v

relative to the total solution [37] or 20% w/w relative to the HPMC content [42]). This concentration was selected to ensure effective ester crosslinking while preserving fiber integrity, as higher citric acid contents are reported to induce fiber brittleness, whereas lower concentrations result in insufficient water resistance [37]. Azelaic acid (0.2% w/w) also was directly dispersed into the mixture prior to electrospinning to ensure uniform incorporation and to prevent premature crosslinking (Table 1). The resulting solution was magnetically stirred until homogeneous and immediately used for electrospinning. For this study, four distinct formulations were prepared to systematically evaluate fiber morphology and develop the final drug-loaded system, as detailed in Table 1.

2.3. Electrospinning process

Each electrospinning solution was loaded into a 10 mL syringe fitted with a 22G stainless steel needle, connected to a digitally controlled syringe pump (Inovenso NE-300, USA), and electrospun onto a grounded cylindrical collector covered with aluminum foil. Processing parameters were optimized for each formulation. For neat HPMC, continuous fibers were obtained at an applied voltage of 11 kV, a tip-to-collector distance of 10 cm, and a feed rate of 0.2 mL/h (in line with previous reports [42]). In contrast, the blended HPMC/PVA formulations containing citric acid and azelaic acid required milder conditions (7 kV, 11.5 cm, and 1.5 mL/h) to achieve stable jets and effective solvent evaporation. For drug-loaded (AzA) solutions, the electrospinning syringe was replenished every 4 h to prevent nozzle clogging and ensure consistent fiber formation. All electrospun mats were vacuum-dried and stored in a desiccator until characterization. To ensure batch-to-batch reproducibility, electrospinning was conducted under controlled environmental conditions (25 ± 2 °C and 35 ± 5% relative humidity). Three independent batches were prepared and processed for the optimized formulation. SEM analysis confirmed consistent fiber morphology and diameter distribution across replicates.

2.4. Crosslinking process

The collected fibers were thermally crosslinked by heating at 140 °C for 1 h. This condition was chosen to activate esterification between the hydroxyl groups of HPMC/PVA and the carboxyl groups of citric acid [43]. Importantly, this temperature is safe for the active ingredient, as pure azelaic acid exhibits thermal stability with an onset of decomposition between 228 and 274 °C [44]. Thermal treatment in this range is widely reported to drive covalent ester bond formation, resulting in a more stable three-dimensional network with improved water resistance and controlled swelling [45,46]. Previous studies have demonstrated that heating above 120 °C is critical to achieve effective crosslinking, while 140–160 °C provides a balance between reaction efficiency and preservation of fiber morphology [43]. Structurally, the crosslinking is driven by Le Chatelier's principle: heating removes water, shifting the esterification equilibrium toward bond formation [45]. Through this thermal crosslinking process, the resulting mats were structurally reinforced without losing their fibrous architecture, supporting their intended application as pH-responsive carriers.

2.5. Surface morphology

The morphology of electrospun fibers was characterized using scanning electron microscopy (SEM, JEOL-6480LV, JEOL Ltd., Japan) after gold sputter coating. SEM was employed to evaluate the influence of HPMC concentration, ethanol–water solvent ratio, and PVA incorporation on fiber uniformity and bead formation. Average fiber diameters were calculated from representative SEM micrographs by measuring at least 50 fibers per sample using ImageJ software.

2.6. Fourier transform infrared spectroscopy

Fourier transform infrared spectroscopy (FTIR, L1600300 Spectrum TWO LiTa, PerkinElmer AES, UK) was used to evaluate the chemical composition and crosslinking of the electrospun mats. Spectra were recorded in the range of 4000–500 cm^{-1}, and characteristic absorbance peaks corresponding to the functional groups of HPMC, PVA, and azelaic acid were identified.

2.7. Thermal properties analysis of HPMC/PVA electrospun fibers

The thermal behavior of the electrospun mats was evaluated using differential scanning calorimetry (DSC Q250, TA Instruments, New Castle, DE, USA). Samples (~5 mg) were sealed in aluminum pans and heated from 50 to 250 °C at a rate of 10 °C/min under a nitrogen atmosphere. The analysis was performed to determine melting temperature, and crystallinity changes associated with polymer blending and citric acid crosslinking.

2.8. Water contact angle

Wettability of the electrospun mats was assessed by static water contact angle (WCA) measurements using a Krüss™ DSA100 goniometer. A 4 μL droplet of deionized water was gently placed on the mat surface at 25 ± 0.5 °C, and the contact angle was recorded immediately. For each sample, measurements were performed at five different positions and averaged to obtain representative values.

2.9. Water uptake and degradation of electrospun mats

The stability and hydrophilicity of the electrospun mats were evaluated through water uptake and degradation studies. For water uptake test, samples were incubated in phosphate-buffered saline (PBS, pH 7.4) at 37 °C under static conditions. At selected time points (from 5 min up to 7 days), mats were removed, gently blotted to eliminate excess surface water, and weighed immediately. The percentage of water uptake was determined according to Formula 1.

$$Water\ uptake\ (\%) = ((Wet\ weight - Dry\ weight) / (Dry\ weight)) \times 100 \quad \text{Eq. 1}$$

Furthermore, degradation or mass loss profile was evaluated from

Table 1
Composition and formulation details of the electrospinning solutions.

Group	Polymers	HPMC Conc. (%w/v)	PVA Conc. (%w/v)	CA (0.5 % w/v) crosslinking	HPMC/PVA solution ratio	AzA (0.2 % w/v) Drug-loaded	Solvents (v/v%)
1	HPMC	1	0	No	100/0	No	50:50 H_2O/EtOH
2	HPMC + PVA	1	8	No	50/50	No	50:50 H_2O/EtOH
3	HPMC + PVA	1	8	No	70/30	No	50:50 H_2O/EtOH
4	HPMC + PVA	1	8	Yes	70/30	Yes	50:50 H_2O/EtOH

the reduction in water uptake over time. After reaching maximum swelling, the mats gradually lost weight, and this decline provided a clear and reliable indication of structural degradation, as illustrated in the corresponding diagrams [47]. These analyses provide key insights into how crosslinking and polymer composition influence mat integrity, swelling, and long-term behavior in physiological environments, which is essential for biomedical [48].

2.10. Evaluation of drug encapsulation efficiency

The encapsulation efficiency (EE%) of AzA within the electrospun fibers was determined to assess the effectiveness of the loading process. Approximately 10 mg of drug-loaded mat was extracted in 10 mL ethanol: water (50:50 v/v) using 30 min sonication followed by 10 min magnetic stirring. Samples were filtered (0.45 μm) and the AzA content was quantified by UV–Vis spectroscopy at 204 nm using a calibration curve. This solvent system ensured the complete dissolution of both the polymeric matrix and the encapsulated AzA. The encapsulation efficiency was calculated using the following equation [49]:

$$EE\% = ((Amount\ of\ drug\ in\ mat) / (Drug\ initially\ added)) \times 100 \quad \text{Eq. 2}$$

Each measurement is carried out in triplicate, and results are reported as the mean value ± standard deviation (SD).

2.11. pH-dependent release of azelaic acid from HPMC/PVA mats

The pH-responsive release behavior of AzA from the electrospun mats was evaluated to demonstrate their potential as a smart drug delivery system. The investigation began by comparing non-crosslinked and crosslinked mats in phosphate-buffered saline (PBS, pH 7.4) to establish the fundamental role of crosslinking in controlling release kinetics. To further probe pH sensitivity, release studies were conducted on crosslinked mats using three model buffers (pH 4.5, 6.0, and 7.4) [9]. These pH values were selected to represent a range of skin conditions, from healthy acidic skin (pH ~5.5) to the elevated pH levels found in pathological states like acne and chronic wounds, which can reach up to 7.4.

In this study, fiber samples (approximately 20 mg) were immersed in 20 mL of the release medium buffers within sealed vials maintained at 37 °C under constant agitation (100 rpm). At predetermined time intervals, aliquots (2 mL) of the release medium were withdrawn and immediately replaced with an equal volume of fresh buffer to maintain sink conditions. The samples were analyzed by UV–Vis spectroscopy at a wavelength of $\lambda = 204$ nm. Furthermore, the properties of azelaic acid are crucial for this study. Its solubility and UV absorption can change with pH because it has two acidic groups ($pKa_1 \approx 4.5$, $pKa_2 \approx 5.3$) that become ionized as pH increases [38,41]. To ensure accurate quantification across the different pH environments, separate calibration curves were constructed for each buffer. The cumulative release of azelaic acid was calculated as a percentage of the actual drug content within each mat, as determined by encapsulation efficiency measurements. All experiments were conducted in triplicate, and the mean values are reported.

2.12. Mathematical modeling of azelaic acid release kinetics

To gain deeper insight into the mechanism of drug release, the experimental data were fitted to several mathematical models. The release profiles were analyzed using zero-order, first-order, and Higuchi models. Furthermore, the Korsmeyer-Peppas model was applied to determine the release exponent (n), which helps identify the dominant drug transport mechanism. The drug release fitting was performed on the initial 60% of release data and interpreted using slab geometry cut-offs [50]. The release exponent identifies the transport mechanism: Fickian diffusion ($n \leq 0.45$), anomalous transport ($0.45 < n < 0.89$), or Case-II transport ($n \geq 0.89$). The best-fit model was selected based on the highest R^2 value [51].

2.13. Statistical analysis

All experiments were performed in triplicate ($n = 3$) unless otherwise stated. Data are presented as mean ± standard deviation (SD). Statistical comparisons between groups were conducted using one-way ANOVA followed by Tukey's post-hoc test, with significance defined as $p < 0.05$. Drug release kinetics were fitted to zero-order, first-order, Higuchi, and Korsmeyer–Peppas models using OriginPro 2024 (OriginLab, USA), and the best-fit model was identified based on the highest coefficient of determination (R^2).

3. Results and discussion

3.1. Morphological analysis of the HPMC/PVA electrospun mats

As shown in Fig. 3a and b, even with ethanol-water co-solvent, the pure HPMC mats (Group 1) exhibited poor morphology, consisting of broken and discontinuous fibers. This confirms that HPMC cannot form uniform fibers independently, consistent with previous reports [52]. Further failed attempts using aqueous HPMC solutions are provided in Supplementary Fig. S1. To overcome this, HPMC was blended with poly (vinyl alcohol) (PVA). A 50:50 HPMC/PVA blend (Group 2) significantly improved fiber continuity, confirming PVA's role as an effective carrier polymer (Fig. 3c and d). However, the optimal and most uniform morphology was achieved in Group 3, with a higher HPMC to PVA ratio (Fig. 3e and f). This superior uniformity is attributed to a more stable electrospinning jet, which was achieved by optimizing the polymer blend's properties. While PVA provides essential chain entanglement, at a high 50/50 ratio (Group 2) its flexible chains can lead to substantial water retention and jet instability, causing fiber fusion and diameter variation [27,28]. In contrast, the increased HPMC fraction in Group 3 (70/30) introduced a critical balance. This ratio was selected to maximize the HPMC content, which serves as the primary drug release matrix, while utilizing the minimum amount of PVA required to ensure spinnability. HPMC's molecular structure, characterized by methoxyl and hydroxypropyl substitutions, imparts greater chain rigidity and promotes faster solvent evaporation compared to PVA [29]. Consequently, the 70/30 blend represents the optimized formulation window where sufficient chain entanglement (provided by PVA) overlaps with the structural stability and rapid solvent evaporation (provided by HPMC) to prevent the fiber fusion observed in the 50/50 blend. This produced a stable electrospinning jet, resulting in uniform, bead-free fibers. Due to this uniform morphology, the Group 3 formulation was selected for all further functional studies [27].

3.2. FTIR spectra of the HPMC/PVA electrospun mats

The FTIR spectra of pure HPMC (group1), HPMC/PVA non-crosslinked (group3), and drug-free HPMC/PVA crosslinked (blank formulation) samples are presented in Fig. 4. Drug-free samples were selected for this analysis to eliminate spectral interference from azelaic acid and strictly evaluate the formation of ester crosslinks. Pure HPMC shows a broad band around 3450 cm^{-1} corresponding to O–H stretching of hydroxyl groups, a peak at 2920 cm^{-1} assigned to C–H stretching of $–CH_2$ groups, and a band near 1060 cm^{-1} related to C–O–C stretching vibrations of the cellulose ether backbone [53]. The non-crosslinked HPMC/PVA blend displays a broader O–H stretching peak near 3400 cm^{-1} compared to pure HPMC, indicating strong intermolecular hydrogen bonding between the hydroxyl groups of HPMC and PVA. The C–H stretching band remains at 2920 cm^{-1}, confirming the preservation of the polymer backbones upon blending [54].

After crosslinking, the FTIR spectrum of HPMC/PVA shows notable changes. The O–H stretching peak around 3400 cm^{-1} becomes less intense, reflecting the consumption of free hydroxyl groups during

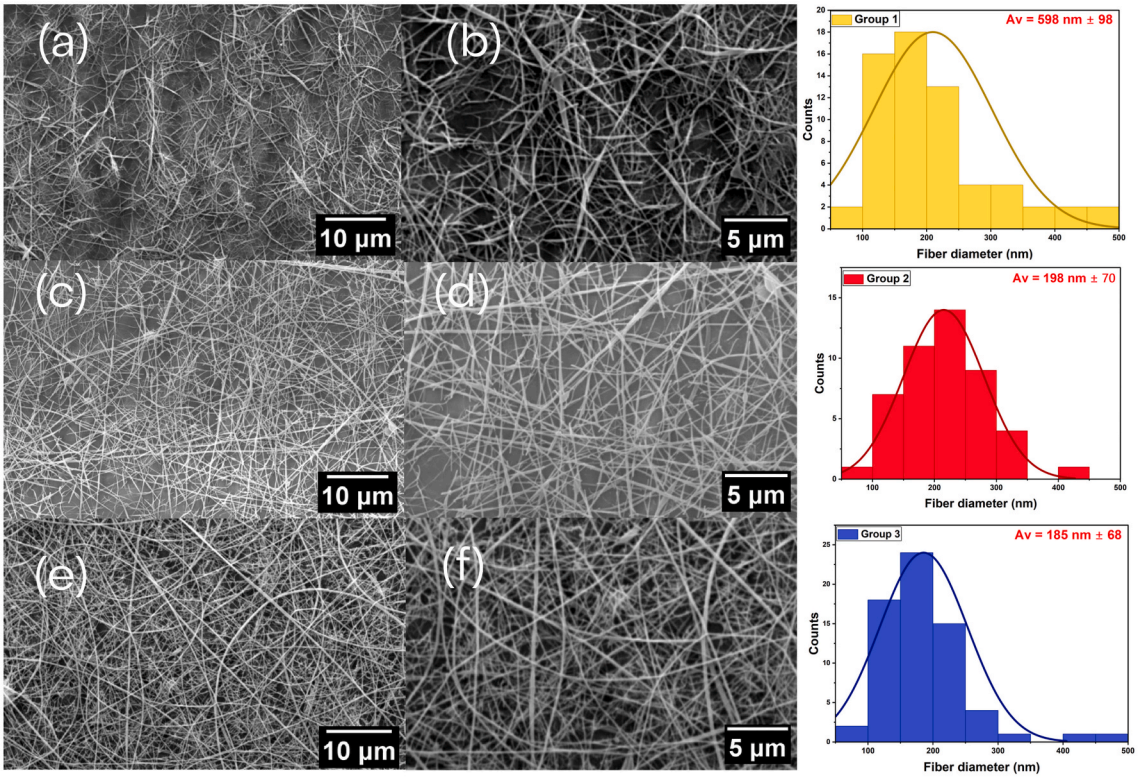

Fig. 3. SEM images at 2000x and 4000x of: (a,b) Pure HPMC (Group 1), (c,d) 50:50 HPMC/PVA (Group 2), and (e,f) Optimized 70/30 HPMC/PVA (Group 3), with corresponding fiber diameter histograms of 50 fibers.

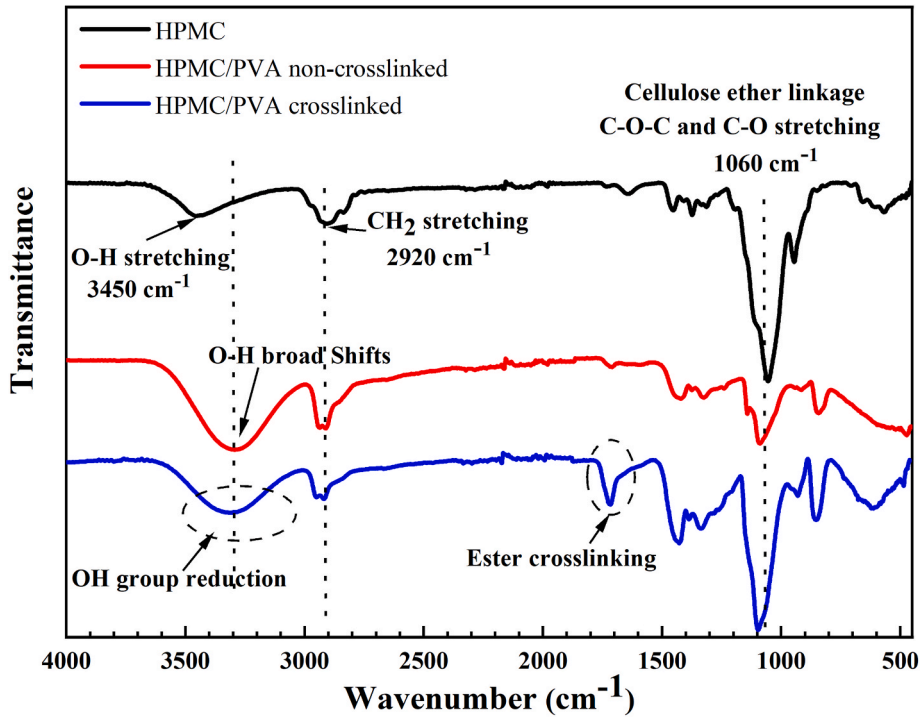

Fig. 4. FTIR spectra of electrospun HPMC, HPMC/PVA non-crosslinked, and HPMC/PVA crosslinked (drug-free).

crosslinking reactions. Crucially, a distinct new peak appears at 1734 cm^{-1}, which is assigned to the ester carbonyl stretching vibration. This assignment is validated by a comparison with pure citric acid and literature standards. While the C=O stretch of pure citric acid typically appears between 1709 cm^{-1} [55] and 1727 cm^{-1} [56] due to hydrogen bonding, the esterification reaction shifts this band to higher wavenumbers. Our observation aligns with previous studies on citric acid-crosslinked HPMC films, which explicitly identify the ester linkage at around 1733 cm^{-1} [37]. Additionally, the band in the 1100–1050 cm^{-1} region corresponding to C–O and C–O–C stretching

shifts slightly, which further indicates modifications in the polymer network [36]. This FTIR confirmation of crosslinking is further supported by the DSC analysis (discussed below), where the absence of the citric acid melting peak confirms that the crosslinker has been chemically integrated into the network rather than remaining as a free acid.

3.3. Differential scanning calorimetry of the electrospun mats

While the thermal properties of pure HPMC (amorphous) and PVA (semi-crystalline) are well-established in the literature [57–59], the DSC thermograms of the non-crosslinked and crosslinked HPMC/PVA mats (Fig. 5) were compared to specifically isolate the effect of citric acid crosslinking. Thermogravimetric degradation of HPMC and PVA typically occurs well above the processing conditions used in this study. Literature reports indicate that HPMC degradation initiates above 210 °C [59], while PVA remains stable up to approximately 230 °C [58], with primary decomposition events occurring between 220 and 300 °C [59]. Since these values are far beyond the curing temperature (140 °C) and the physiological range relevant to dermatological applications, DSC was selected as the primary thermal technique to evaluate crosslinking-induced phase behavior and drug–polymer interactions.

The DSC result reveals distinct thermal behaviors depending on the crosslinking state. The non-crosslinked HPMC/PVA mat shows a sharp endothermic peak at around 205 °C, which corresponds to the melting of crystalline PVA, while HPMC remains largely amorphous [57,60,61] and therefore does not display a distinct melting peak. This behavior is consistent with previous studies showing that HPMC contributes only a weak glass transition in the 160–190 °C range, whereas PVA, due to its semi-crystalline nature, exhibits a clear melting transition [58]. Blending with amorphous HPMC slightly reduces the crystallinity of PVA, lowering the enthalpy of melting compared with neat PVA [59].

In contrast, the crosslinked sample shows a broader melting peak shifted to a higher temperature (~214 °C). The baseline also gradually rises, indicating changes in the polymer's heat capacity. The broadening and upward shift of the PVA melting transition indicate disruption of regular crystallites and restricted chain mobility due to the formation of covalent ester linkages during citric acid crosslinking [59]. The continuous rise in the baseline is attributed to bound water release and increased heat capacity of the crosslinked network, which further supports the presence of intermolecular anchoring and reduced segmental flexibility [62]. Similar DSC results of broadened and shifted melting peaks after citric acid treatment have been reported in PVA-based membranes and blend films [59]. Taking together, the DSC results confirm that crosslinking reduces crystalline perfection and enhances thermal stability of the HPMC/PVA network.

3.4. Water contact angle

The HPMC/PVA fibers showed moderate wettability before curing, with a water contact angle of 37.3°, as shown in Fig. 6. This value is in good agreement with previous reports on HPMC/PVA film blends, where contact angles of ~35–56° were measured [63], while neat HPMC films show much higher values (~61.8°) due to their lower surface polarity [24]. The incorporation of PVA is therefore known to enhance the hydrophilicity of HPMC-based systems, which is consistent with our results [63].

On the other hand, interestingly, after crosslinking with citric acid, the contact angle of our fibrous mats decreased dramatically to 16.3°, indicating a much more hydrophilic surface. This finding is consistent with previous reports on other polysaccharide-based systems. For instance, CA crosslinking disrupted the crystalline regions of HPMC-NaCMC (sodium carboxymethylcellulose) films, making them more amorphous and easier for water to penetrate. This structural change, combined with the introduction of additional carboxyl (–COOH) groups, increased surface wettability and promoted droplet spreading, leading to a lower contact angle [36]. Likewise, Almeida et al. [64] observed that bacterial cellulose membranes crosslinked with CA exhibited a large decrease in contact angle (from around 77° to 44°), attributed to higher water uptake, increased accessibility of polar groups, and preserved porous structure.

As a result, the decrease in contact angle after CA crosslinking indicates a significant improvement in surface wettability, which is particularly valuable for promoting interaction with biological fluids in skin and dermal applications. Enhanced hydrophilicity and stability

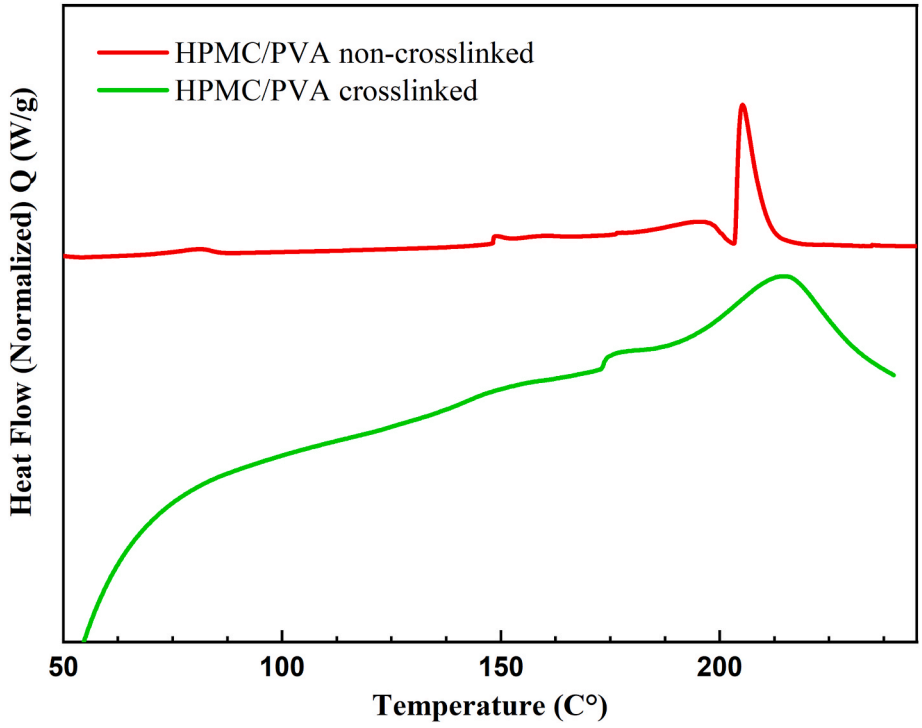

Fig. 5. Thermal curves of HPMC/PVA non-crosslinked, and HPMC/PVA crosslinked.

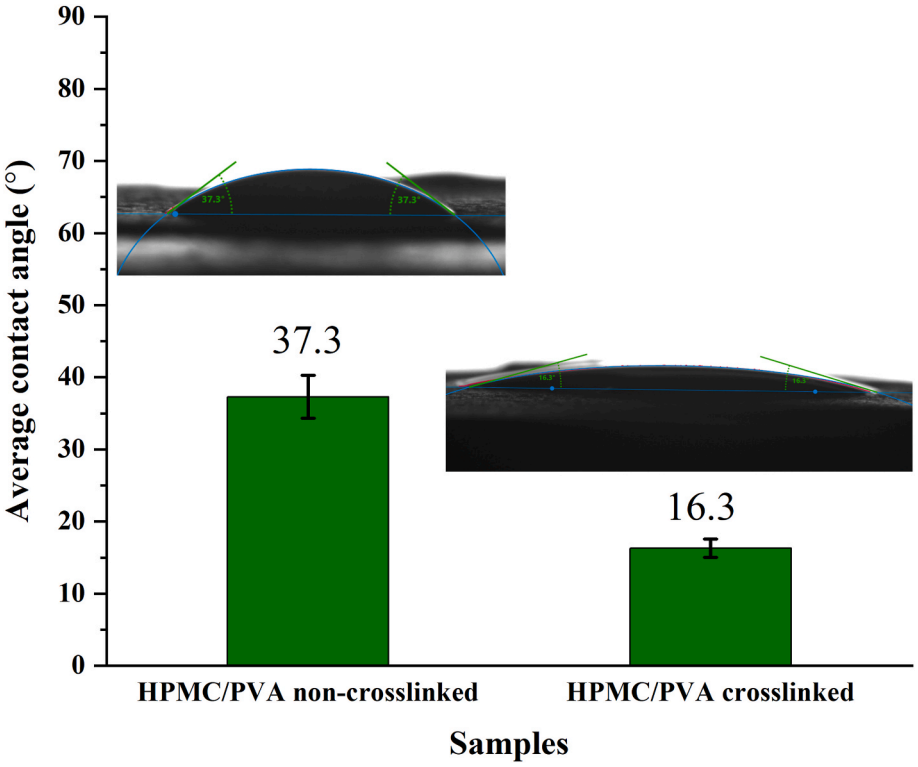

Fig. 6. Water contact angles (WCA) of HPMC/PVA non-crosslinked, and HPMC/PVA crosslinked. (Data are presented as mean ± SD (n = 3). Statistically significant differences ($p < 0.05$) are indicated.).

through CA crosslinking have also been shown to benefit other biomedical applications, such as wound dressings and drug delivery systems, where improved water affinity and structural integrity are critical for therapeutic performance [64].

3.5. Water uptake and degradation of the electrospun mats

All samples were immersed in PBS to evaluate their water uptake and degradation profile under simulated physiological conditions [65]. To allow for accurate comparison between samples, all data was

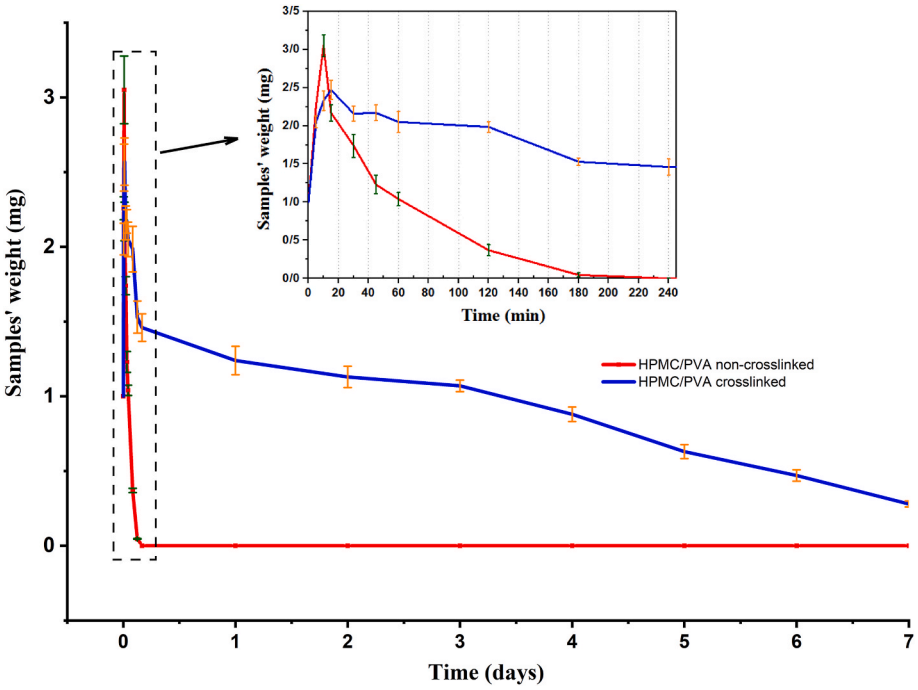

Fig. 7. Water uptake and in vitro degradation of 1 mg normalized samples of HPMC/PVA nanofibers (non-crosslinked and citric acid crosslinked). Water uptake was recorded at 5, 10, 15, 30, 45, 60, 120, 180, and 240 min, while degradation of crosslinked samples was monitored over a period of 7 days. (Data are presented as mean ± SD (n = 3). Statistically significant differences ($p < 0.05$) are indicated.).

normalized. The wet weight of each mat at each time point was divided by its initial dry mass. The results in Fig. 7 are presented as normalized to a 1 mg starting mass. Changes were monitored over both short-term (minutes to hours) and long-term (days) immersion. The degradation rate of fibrous biomaterials is important: fast-degrading mats are useful for drug release and short-term skin dressings, while slow-degrading mats are better for maintaining structure in long-term scaffolds or dermal supports [32].

In previous studies, HPMC polymer typically absorbed around 100% of their weight in water within the first hour [66,67]. While pure PVA mats showed much higher uptake, reaching up to 500% within 30 min, and then rapidly disintegrated because of their high solubility and lack of hydrophobic domains [68]. Building on this, the non-crosslinked HPMC/PVA mats exhibited very rapid hydration, with water uptake reaching around 210% of the original mass within just 10 min, before undergoing rapid dissolution and complete degradation by 180 min. This profile is consistent with the high hydrophilicity and water solubility of both HPMC and PVA when not stabilized by crosslinks [35].

In contrast, CA crosslinked HPMC/PVA mats showed a much slower and more controlled hydration–degradation profile. As shown in Fig. 7, blue line, swelling peaked at about 155% after 15 min, and degradation proceeded more slowly, with approximately 28% of the initial mass remaining after 7 days (Visual observations at 1 and 7 days are shown in Supplementary Fig. S2. This difference is attributed to ester bond formation between CA carboxyls and polymer hydroxyls, which creates a denser, more stable network that resists rapid dissolution while still allowing water penetration [69]. Several reports confirm that CA-crosslinked polysaccharide or PVA systems display enhanced resistance to hydrolysis, slower degradation kinetics, and improved stability in aqueous environments [70]. This stabilization, together with the increase in hydrophilicity (lower contact angle) observed in our study, provides an important advantage: the mats stay highly wettable and interact well with skin fluids while maintaining their structure, making them especially promising for dermal drug delivery, wound dressings, and biomedical patches.

3.6. pH-dependent release of azelaic acid from HPMC/PVA mats

The drug release profiles provide compelling evidence of a successfully engineered pH-responsive system, highlighted by the profound, pH-gated behavior of crosslinked mats across the physiological pH range. At pH 4.5, simulating the minimum acidic environment of healthy skin, the release of AzA from these mats was exceptionally slow and minimal, with negligible cumulative release detected over 24 h. This finding was further corroborated by the UV-Vis analysis (Fig. S3), which confirmed the absence of a characteristic azelaic acid absorption peak after 24 h, validating the negligible drug release at this pH. Two key factors caused this strong suppression: First, at acidic pH, the crosslinked network stays tightly packed. This happens because the carboxyl groups are protonated (-COOH) and form strong hydrogen bonds, which locks the structure and prevents swelling [71,72]. Second, at this acidic pH (4.5), azelaic acid itself ($pKa_1 \approx 4.5$, $pKa_2 \approx 5.3$) exists largely in its neutral, lipophilic form (AH_2). This form exhibits very low aqueous solubility, thus minimizing the concentration gradient that drives diffusion [73].

On the other hand, as shown in Fig. 8, the release kinetics are governed by a precise interplay between the swelling of the crosslinked fiber matrix and the pH-dependent ionization of the polymer network and azelaic acid drug molecule. As the pH increases to 6.0, a condition relevant to mild or early stages of skin issues, the release profile transitions to an intermediate state, reaching approximately 21% after 96 h (Fig. 8a). This transition to an intermediate state is a critical finding, as it demonstrates the system's graduated response to pH rather than a simple on/off switch. At this pH, which is near the pKa values of both the azelaic acid ($pKa_2 \approx 5.3$) and the carboxyl groups in the citric acid-crosslinked network, both the drug and the matrix undergo partial ionization. This induces a moderate degree of electrostatic repulsion within the matrix, leading to measurable swelling, and increases the solubility of AzA, resulting in a balanced, sustained release rate [74,75].

The most rapid and extensive release occurred at pH 7.4, simulating diseased skin states like chronic wounds or eczema [9], where the cumulative release increased to over 87% within 96 h. Under these conditions, the carboxyl groups on the citric acid crosslinks are fully deprotonated ($-COO^-$) as shown in Fig. 9, generating strong electrostatic repulsion that forces the network to swell dramatically, creating large aqueous channels for drug diffusion [75]. Concurrently, azelaic acid undergoes progressive ionization to its highly soluble di-anionic form (A^{2-}) at pH 7.4, increasing the thermodynamic driving force for diffusion. This confirms that the release behavior is drug-matrix coupled rather than purely matrix-controlled, arising from the synergistic interplay between polymer network swelling and pH-dependent drug ionization [73]. On the other hand, the fundamental role of chemical crosslinking is vividly illustrated by comparing crosslinked and non-crosslinked mats at pH 7.4 (Fig. 8b). The non-crosslinked fibers exhibited a rapid burst release, with over 92.6% of the drug liberated within 2 h. This is characteristic of a dissolution-controlled system, where the water-soluble HPMC and PVA blend disintegrates upon contact with the aqueous medium [76].

3.7. Model fitting results and interpretation

The release data were fitted to zero-order, first-order, and Higuchi models (see Supplementary Table S1 for detailed parameters). However, the Korsmeyer-Peppas model provided the best fit, as indicated by the

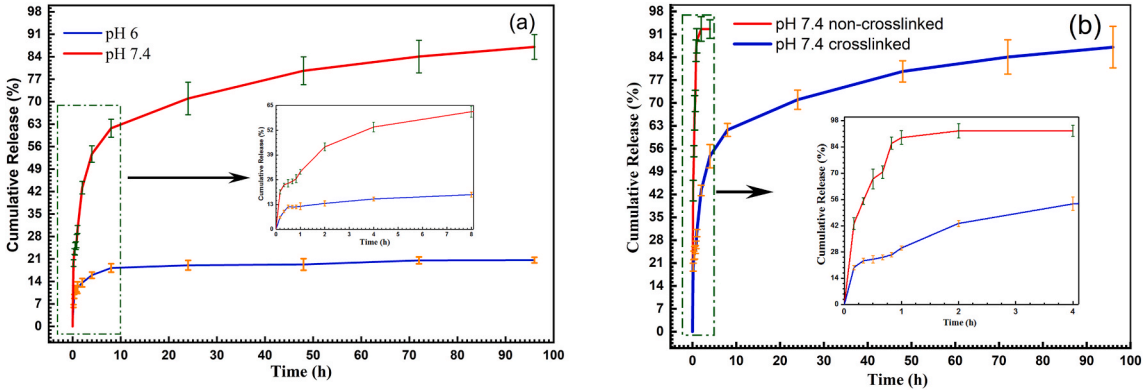

Fig. 8. pH-dependent release of azelaic acid from electrospun fiber mats. (a) Cumulative release from citric acid-crosslinked HPMC/PVA mats at pH 6.0 and pH 7.4, demonstrating sustained and pH-triggered release. (b) Comparison of release profiles at pH 7.4 for crosslinked versus non-crosslinked mats. (Data are presented as mean ± SD (n = 3). Statistically significant differences ($p < 0.05$) are indicated.).

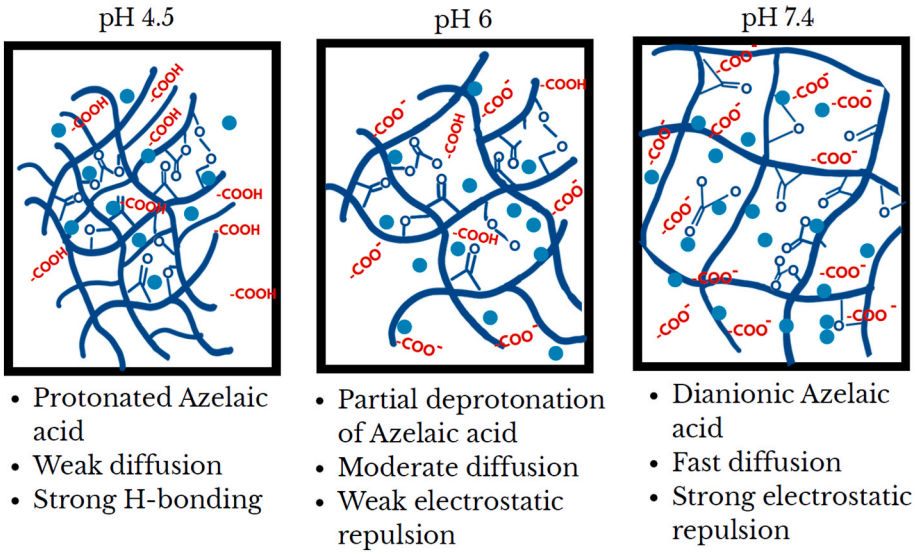

Fig. 9. Schematic diagram illustrating the proposed pH-dependent release mechanism, linking polymer network swelling and azelaic acid ionization state at pH 4.5, 6.0, and 7.4.

highest correlation coefficients ($R^2 > 0.92$), and was therefore selected for a detailed analysis of the release mechanism. This model is particularly suited for polymeric systems where both diffusion and swelling play a role [77]. The drug transport mechanisms were further investigated by fitting the release data from the crosslinked mats (pH 6.0 and 7.4) to the Korsmeyer-Peppas model. Kinetic analysis at pH 4.5 was not possible due to the negligible drug release. Also, the raw release data and the detailed numerical calculations used for the Korsmeyer-Peppas model fitting are provided in Supplementary Table S2.

The Korsmeyer-Peppas model is described by the equation:

$$M_t / M_\infty = K.t^n \quad \text{Eq. 3}$$

where M_t/M_∞ is the fraction of drug released at time t, k is the release rate constant, and n is the release exponent that indicates the transport mechanism.

The fitted parameters are summarized in Table 2. The high correlation coefficients ($R^2 > 0.92$) confirm that the Korsmeyer-Peppas model provides a good fit to the release data.

The release exponent provides critical insight into the drug transport mechanism. For both pH 6.0 and pH 7.4, the n values of 0.28 and 0.45, respectively, are less than or equal to 0.45, indicating that Fickian diffusion is the primary release mechanism [78,79]. In this regime, drug release is governed primarily by the concentration gradient, consistent with Fickian diffusion. However, considering the pronounced pH-dependent swelling, the polymer chains are not strictly static; instead, diffusional transport dominates while being facilitated by swelling-induced structural relaxation of the network. However, the clear increase in the release exponent from 0.28 to 0.45, coupled with the 2.5-fold increase in the release rate constant k, reveals important pH-dependent behavior. While diffusion remains the dominant mechanism, the higher pH environment enhances the drug transport process.

Table 2
Parameters of the Korsmeyer-Peppas model for azelaic acid release from crosslinked HPMC/PVA mats (fitted for the first 60% of release).

pH	Release rate constant (k) ($time^{-n}$)	Release exponent (n)	R^2	Release mechanism
6.0	12.30 ± 0.85	0.28 ± 0.03	0.92	Fickian Diffusion
7.4	30.20 ± 1.25	0.45 ± 0.02	0.98	Fickian Diffusion

This acceleration can be attributed to the increased swelling of the polymer matrix at pH 7.4, which creates a more porous and hydrated structure through which the ionized azelaic acid can diffuse more rapidly [80]. The fact that the release at pH 4.5 was too slow to model quantitatively serves as the strongest evidence for the critical role of pH-responsive swelling in controlling drug release from this system. Mathematical modeling thus confirms that while the fundamental mechanism is diffusion-based, the rate of diffusion is profoundly enhanced by the pH-triggered swelling of the citric acid-crosslinked network.

4. Conclusion and future perspectives

In conclusion, this study successfully demonstrates a safe and effective strategy for targeted drug delivery by chemically transforming the cellulose derivative HPMC into a pH-sensitive platform. We addressed the inherent limitations of electrospinning pure HPMC (poor spinnability/water solubility) by optimizing the solvents, polymer concentration, and electrospinning process to ensure uniform fiber formation. The critical step of citric acid crosslinking then transformed this hydrophilic carbohydrate blend into a robust, water-resistant platform, as demonstrated by its 7-day stability in the in vitro degradation study. The successful chemical modification was further confirmed by DSC analysis (which showed enhanced thermal stability) and a marked reduction in water contact angle, which signifies superior wettability for biological interaction. The resulting mat exhibited a powerful "smart" release profile, shifting from a rapid, uncontrolled burst (over 90% in 2 h) to a precisely controlled, pH-triggered release. Kinetic modeling confirmed that drug transport is governed by Fickian diffusion, with the release rate profoundly accelerated by pH-triggered swelling. This system successfully discriminated between physiological conditions, showing minimal release at healthy skin pH (4.5) and maximum release (over 87% in 96 h) at the higher pH of diseased skin. This demonstrated potential to provide on-demand drug release in response to specific biological triggers is the core achievement of this work.

Looking forward, this versatile fibrous platform establishes a promising and scalable foundation for the next generation of topical therapies. It can be readily adapted for a wide range of other pH-sensitive therapeutics, opening new avenues for treating conditions like chronic wounds, acne, and eczema with improved stability and enhanced efficacy. However, to fully realize this clinical potential, future work will focus on conducting in vitro cytotoxicity assays and ex vivo skin

permeation studies to validate the safety and biological performance of these intelligent fibers.

Declaration of generative AI and AI-assisted technologies in the manuscript preparation process

During the preparation of this work the authors used Gemini in order to assist with language refinement and structural organization. After using this tool, the authors reviewed and edited the content as needed and take full responsibility for the content of the published article.

Funding

The authors acknowledge the financial support provided by the Natural Sciences and Engineering Research Council of Canada (NSERC), grant number ALLRP 584745-23.

CRediT authorship contribution statement

Ehsan Niknejad: Conceptualization, Investigation, Methodology, Writing – original draft. **Reza Jafari:** Funding acquisition, Project administration, Supervision, Writing – review & editing. **Valeria Morales Pascal:** Formal analysis, Investigation, Writing – review & editing. **Gelareh Momen:** Resources, Supervision.

Declaration of competing interest

The authors declare that they have no known competing financial interests or personal relationships that could have appeared to influence the work reported in this paper.

Acknowledgments

This work was supported by NSERC, CREPEC, Be-UP biotechnology, Alkegen, Prima-Quebec, Cimagi, CISD.

Appendix A. Supplementary data

Supplementary data to this article can be found online at https://doi.org/10.1016/j.jddst.2026.108113.

Data availability

Data will be made available on request.

References

[1] V. Tayebi-Khorrami, et al., Advanced applications of smart electrospun nanofibers in cancer therapy: with insight into material capabilities and electrospinning parameters, Int. J. Pharm. X 8 (2024) 100265.
[2] S. Nikitha, D. Manjula, A. Nasrine, Advances in pH-Sensitive polymer-based drug delivery systems for targeted therapy in ovarian cancer: focus on olaparib, J. Drug Deliv. Sci. Technol. 111 (2025) 107076.
[3] X. Zhou, et al., Development of cationic pH-sensitive liposomes with gemcitabine loading and Fucoidan-coating against pancreatic cancer cells, J. Drug Deliv. Sci. Technol. 100 (2024) 106035.
[4] L. Wei, et al., Preparation of antibacterial/antiviral and pH responsive nanofiber membranes based on cellulose acetate, J. Polym. Res. 32 (2) (2025) 52.
[5] A. Arnaiz, et al., Naked-eye detection of Legionella pneumophila using smart fluorogenic polymers prepared as hydrophilic films, coatings, and electrospun nanofibers, Sensor. Actuator. B Chem. 425 (2025) 136976.
[6] J. Singh, P. Nayak, pH-responsive polymers for drug delivery: trends and opportunities, J. Polym. Sci. 61 (22) (2023) 2828–2850.
[7] D.J. Panther, S.E. Jacob, The importance of acidification in atopic eczema: an underexplored avenue for treatment, J. Clin. Med. 4 (5) (2015) 970–978.
[8] N. Bharti, et al., Smart microneedle platforms for skin cancer therapy: a review of stimuli-responsive and targeted drug delivery systems, Pharmaceut. Dev. Technol. (2025) 1–36.
[9] K. Rizi, et al., Using pH abnormalities in diseased skin to trigger and target topical therapy, Pharm. Res. 28 (10) (2011) 2589–2598.
[10] M.D. Markovic, et al., Status and future scope of hydrogels in wound healing, J. Drug Deliv. Sci. Technol. 98 (2024) 105903.
[11] E. Niknejad, R. Jafari, N. Valipour, Motlagh *mechanical properties of biodegradable fibers and fibrous mats: a comprehensive review*, Molecules 30 (2025) 3276, https://doi.org/10.3390/molecules30153276.
[12] A. Miki, et al., Development of a solid dispersion system for polyvinyl alcohol nanofibers embedded with silicon dioxide particles via emulsion electrospinning for improved solubility of poorly water-soluble drugs, J. Drug Deliv. Sci. Technol. 99 (2024) 105915.
[13] E. Tayerani, et al., Electrospun chitosan nanofibers for tissue engineering, in: 14th IEEE International Conference on Nanotechnology, 2014.
[14] O. Yavuz, et al., Design and evaluation of novel poly (vinyl alcohol)-based electrospun nanofibers bearing quaternized zinc phthalocyanine with improved antibacterial efficiency, J. Environ. Chem. Eng. 13 (6) (2025) 119744.
[15] H. Azizi, A. Koocheki, B. Ghorani, Controlled release and enhanced bioavailability of curcumin using multilayered LPSG/PVA and zein/gluten nanofibers fabricated by emulsion electrospinning, Food Chem. 492 (2025) 145558.
[16] T.R. Rêgo, A.L. Toledo, M.L. Dias, Effect of processing on the morphology and structure of PLGA/PVA fibers produced by coaxial electrospinning, Processes 13 (2025) 1837, https://doi.org/10.3390/pr13061837.
[17] I. Gunderen, et al., An innovative synergy between metal-free click reaction and electrospinning for the fabrication of sustainable Castor oil-modified poly (vinyl chloride) cross-linked nanofiber scaffolds, J. Environ. Chem. Eng. 13 (5) (2025) 118551.
[18] J. Schoeller, et al., pH-Responsive electrospun nanofibers and their applications, Polym. Rev. 62 (2) (2022) 351–399.
[19] H. Alipour, et al., Anti-melanogenic activity of vanadium incorporated PVA chitosan electrospun fibers: an in vitro model, J. Drug Deliv. Sci. Technol. 75 (2022) 103644.
[20] E.T. Nicknejad, S.M. Ghoreishi, N. Habibi, Electrospinning of cross-linked magnetic chitosan nanofibers for protein release, AAPS PharmSciTech 16 (6) (2015) 1480–1486.
[21] E. Mavrokefalou, et al., Preparation and in vitro evaluation of electrospun sodium alginate fiber films for wound healing applications, J. Drug Deliv. Sci. Technol. 81 (2023) 104298.
[22] U. Sampath, T.M. Gunathilake, et al., pH-responsive poly(lactic acid)/sodium carboxymethyl cellulose film for enhanced delivery of curcumin in vitro, J. Drug Deliv. Sci. Technol. 58 (2020) 101787.
[23] W. Pinket, et al., Hydroxypropyl methylcellulose phthalate films reinforced with nanocrystalline cassava starch and intended its applications for colonic drug delivery, J. Drug Deliv. Sci. Technol. 98 (2024) 105908.
[24] A.M. Alghamdi, *Fabrication and comprehensive characterization of HPMC/PVA/CMC-MoO_3 bio-nanocomposites: enhanced mechanical, electrical, and antibacterial properties for food packaging applications*, Int. J. Biol. Macromol. 287 (2025) 138612.
[25] S.M. Mortazavi, N.Z. Chamgordani, S.A. Mortazavi, A comparison between solvent casting and electrospinning methods for the fabrication of HPMC fast-dissolving films: investigation of the physicochemical, mechanical and drug release characteristics, Phys. Scri. 99 (6) (2024) 065906.
[26] J. Bodillard, et al., Functionalisation of polysaccharides for the purposes of electrospinning: a case study using HPMC and Si-HPMC, Gels 1 (1) (2015) 44–57.
[27] T.P. Lodge, et al., Gelation, phase separation, and fibril formation in aqueous hydroxypropylmethylcellulose solutions, Biomacromolecules 19 (3) (2018) 816–824.
[28] M.A. Teixeira, M.T.P. Amorim, H.P. Felgueiras, Poly(Vinyl Alcohol)-Based nanofibrous electrospun scaffolds for tissue engineering applications, Polymers 12 (1) (2020) 7.
[29] G. Akhouy, et al., Recent applications on biopolymers electrospinning: strategies, challenges and way forwards, Polymer-Plastics Technology and Materials 62 (13) (2023) 1754–1775.
[30] D. Sharma, F.M. Harte, G.R. Ziegler, Fabrication and physicomechanical performance of casein-hydroxypropyl methylcellulose nanofibers, J. Colloid Interface Sci. 693 (2025) 137601.
[31] U. Paaver, et al., Electrospun nanofibers as a potential controlled-release solid dispersion system for poorly water-soluble drugs, Int. J. Pharm. 479 (1) (2015) 252–260.
[32] S. Chao, et al., Synthesis and characterization of tigecycline-loaded sericin/poly (vinyl alcohol) composite fibers via electrospinning as antibacterial wound dressings, J. Drug Deliv. Sci. Technol. 44 (2018) 440–447.
[33] E. Niknejad, R. Jafari, G. Momen, Electrospun poly(3-hydroxybutyrate-co-3-hydroxyvalerate)/poly(vinyl alcohol) nanofibers prepared via a DMSO–water co-solvent and freeze–thaw crosslinking, J. Mater. Sci. (2025).
[34] A. Kazsoki, P. Szabó, R. Zelkó, Prediction of the hydroxypropyl cellulose—poly (vinyl alcohol) ratio in aqueous solution containing papaverine hydrochloride in terms of drug loaded electrospun fiber formation, J. Pharmaceut. Biomed. Anal. 138 (2017) 357–362.
[35] V.S. Ghorpade, A.V. Yadav, R.J. Dias, Citric acid crosslinked cyclodextrin/hydroxypropylmethylcellulose hydrogel films for hydrophobic drug delivery, Int. J. Biol. Macromol. 93 (2016) 75–86.
[36] K. Dharmalingam, R. Anandalakshmi, Fabrication, characterization and drug loading efficiency of citric acid crosslinked NaCMC-HPMC hydrogel films for wound healing drug delivery applications, Int. J. Biol. Macromol. 134 (2019) 815–829.
[37] P.L. Marani, G.D. Bloisi, D.F.S. Petri, Hydroxypropylmethyl cellulose films crosslinked with citric acid for control release of nicotine, Cellulose 22 (6) (2015) 3907–3918.
[38] X. Feng, et al., Azelaic acid: mechanisms of action and clinical applications, Clin. Cosmet. Invest. Dermatol. 17 (2024) 2359–2371, null.

[39] R. Puleio, et al., Effect of actively targeted copolymer coating on solid tumors eradication by gold nanorods-induced hyperthermia, Int. J. Pharm. 587 (2020) 119641.
[40] A.-G. Petrovici, et al., A comprehensive review of azelaic acid pharmacological properties, clinical applications, and innovative topical formulations, Pharmaceuticals 18 (9) (2025) 1273.
[41] J. Chen, et al., Electrospun biomaterials for scarless acne wound healing: advances and prospects, J. Funct. Biomater. 16 (9) (2025) 316.
[42] Y. Zhang, C. Zhang, Y. Wang, Recent progress in cellulose-based electrospun nanofibers as multifunctional materials, Nanoscale Adv. 3 (21) (2021) 6040–6047.
[43] D. Nataraj, R. Reddy, N. Reddy, Crosslinking electrospun poly (vinyl) alcohol fibers with citric acid to impart aqueous stability for medical applications, Eur. Polym. J. 124 (2020) 109484.
[44] G.T. Nguyen, et al., Azelaic acid/expanded graphite composites with high latent heat storage capacity and thermal conductivity at medium temperature, ACS Omega 6 (12) (2021) 8469–8476.
[45] N. Reddy, Y. Yang, Citric acid cross-linking of starch films, Food Chem. 118 (3) (2010) 702–711.
[46] P.G. Seligra, et al., Biodegradable and non-retrogradable eco-films based on starch–glycerol with citric acid as crosslinking agent, Carbohydr. Polym. 138 (2016) 66–74.
[47] J. Esmaeili, et al., Developing models to predict mechanical behavior of PCL/PHBV composites for tissue engineering: a response surface methodology study, J. Mech. Behav. Biomed. Mater. 173 (2026) 107232.
[48] A. Cordoba, et al., Electrospun bioactive fibers of PCL/starch loaded with bioglass nanoparticles with potential application in bone tissue engineering: an in vitro and in vivo study, J. Drug Deliv. Sci. Technol. 114 (2025) 107496.
[49] D. Honarmand, et al., Controlled release of protein from magnetite–chitosan nanoparticles exposed to an alternating magnetic field, J. Appl. Polym. Sci. 133 (17) (2016).
[50] H.M. Hashem, et al., Fabrication and characterization of electrospun nanofibers using biocompatible polymers for the sustained release of venlafaxine, Sci. Rep. 12 (1) (2022) 18037.
[51] E. Vatankhah, Rosmarinic acid-loaded electrospun nanofibers: in vitro release kinetic study and bioactivity assessment, Eng. Life Sci. 18 (10) (2018) 732–742.
[52] A. Balogh, et al., AC and DC electrospinning of hydroxypropylmethylcellulose with polyethylene oxides as secondary polymer for improved drug dissolution, Int. J. Pharm. 505 (1) (2016) 159–166.
[53] K. Sari, et al., Characterization of citric acid-crosslinked chitosan and hydroxypropyl methylcellulose blended film for coating Cavendish bananas, Int. J. Biol. Macromol. 322 (2025) 146948.
[54] N. Thungphotrakul, P. Prapainainar, Development of polyvinyl alcohol/carboxymethylcellulose-based bio-packaging film with citric acid crosslinking and clove essential oil encapsulated chitosan nanoparticle pickering emulsion, Int. J. Biol. Macromol. 282 (2024) 137223.
[55] R. Shi, et al., Characterization of citric acid/glycerol co-plasticized thermoplastic starch prepared by melt blending, Carbohydr. Polym. 69 (4) (2007) 748–755.
[56] S.-M. Huang, et al., Effect of citric acid on swelling resistance and physicochemical properties of post-crosslinked electrospun polyvinyl alcohol fibrous membrane, Polymers 15 (7) (2023) 1738.
[57] S.E. Bianchi, et al., Evaluation of the solubility of the HPMC: PVA blends in biological fluids in vitro, Mater. Res. 14 (2011) 166–171.
[58] B.J. Holland, J.N. Hay, The thermal degradation of poly(vinyl alcohol), Polymer 42 (16) (2001) 6775–6783.
[59] N.A. Abdel-Zaher, M.T.H. Moselhey, O.W. Guirguis, Effect of fast neutrons on the structure and thermal properties of PVA/HPMC blends, J. Therm. Anal. Calorim. 126 (3) (2016) 1289–1299.
[60] H.R. Luthfianti, et al., Physicochemical characteristics and antibacterial activities of freeze-thawed polyvinyl alcohol/andrographolide hydrogels, ACS Omega 8 (3) (2023) 2915–2930.
[61] H. McPhillips, et al., Characterisation of the glass transition of HPMC using modulated temperature differential scanning calorimetry, Int. J. Pharm. 180 (1) (1999) 83–90.
[62] C. Tsioptsias, et al., Thermal behavior of poly (vinyl alcohol) in the form of physically crosslinked film, Polymers 15 (8) (2023) 1843.
[63] J. Huang, et al., Functional characteristics improvement by structural modification of hydroxypropyl methylcellulose modified polyvinyl alcohol films incorporating roselle anthocyanins for shrimp freshness monitoring, Int. J. Biol. Macromol. 162 (2020) 1250–1261.
[64] A.P.C. Almeida, et al., Crosslinked bacterial cellulose hydrogels for biomedical applications, Eur. Polym. J. 177 (2022) 111438.
[65] A. Iranpour Mobarakeh, et al., Fabrication and evaluation of a bi-layered electrospun PCL/PVA patch for wound healing: release of vitamins and silver nanoparticle, Heliyon 10 (12) (2024) e33178.
[66] V. Michailova, et al., Water uptake and relaxation processes in mixed unlimited swelling hydrogels, Int. J. Pharm. 209 (1-2) (2000) 45–56.
[67] V. Michailova, et al., Influence of hydrogel structure on the processes of water penetration and drug release from mixed hydroxypropylmethyl cellulose/thermally pregelatinized waxy maize starch hydrophilic matrices, Int. J. Pharm. 222 (1) (2001) 7–17.
[68] A.C. Santos, et al., Beyond the surface area: the effect of electrospinning versus casting on molecular packing and its impact on the production of efficient PVA-pectin-Fe adsorbents, Int. J. Biol. Macromol. 332 (2025) 148565.
[69] S. Nangare, et al., Pharmaceutical applications of citric acid, Future J. Pharmaceut. Sci. 7 (1) (2021) 54.
[70] H. Nasution, et al., Hydrogel and effects of crosslinking agent on cellulose-based hydrogels: a review, Gels 8 (9) (2022) 568.
[71] A.S. Hoffman, Hydrogels for biomedical applications, Adv. Drug Deliv. Rev. 64 (2012) 18–23.
[72] N.A. Peppas, A.R. Khare, Preparation, structure and diffusional behavior of hydrogels in controlled release, Adv. Drug Deliv. Rev. 11 (1) (1993) 1–35.
[73] J.R. Fernández, et al., N-Succinyl-S-Farnesyl-L-Cysteine (SFC): a novel isoprenylcysteine analog with in vitro anti-inflammatory activity and clinical skin protecting properties, Cosmetics 8 (4) (2021) 110.
[74] Y. Qiu, K. Park, Environment-sensitive hydrogels for drug delivery, Adv. Drug Deliv. Rev. 53 (3) (2001) 321–339.
[75] D. Schmaljohann, Thermo- and pH-responsive polymers in drug delivery, Adv. Drug Deliv. Rev. 58 (15) (2006) 1655–1670.
[76] J. Siepmann, F. Siepmann, Modeling of diffusion controlled drug delivery, J. Contr. Release 161 (2) (2012) 351–362.
[77] J. Esmaeili, et al., Reliable kinetics for drug delivery with a microfluidic device integrated with the dialysis bag, Mol. Pharm. 20 (2) (2023) 1129–1137.
[78] P.L. Ritger, N.A. Peppas, A simple equation for description of solute release II. Fickian and anomalous release from swellable devices, J. Contr. Release 5 (1) (1987) 37–42.
[79] J. Siepmann, N.A. Peppas, Higuchi equation: derivation, applications, use and misuse, Int. J. Pharm. 418 (1) (2011) 6–12.
[80] N.A. Peppas, J.J. Sahlin, A simple equation for the description of solute release. III. Coupling of diffusion and relaxation, Int. J. Pharm. 57 (2) (1989) 169–172.